ASTRONOMY
AND
ASTROPHYSICS

A radio-continuum and photoionization-model study of the two planetary nebulae in the Sagittarius dwarf galaxy

G. Dudziak[1], D. Péquignot[2], A. A. Zijlstra[3], and J. R. Walsh[4]

[1] Department of Physics and Applied Physics, University of Strathclyde, Scotland. E-mail: gregory.dudziak@strath.ac.uk
[2] Laboratoire d'Astrophysique Extragalactique et de Cosmologie associé au CNRS (UMR 8631) et à l'Université Paris 7, DAEC, Observatoire de Paris-Meudon, F-92195 Meudon Principal Cedex, France. Email: daniel.pequignot@obspm.fr
[3] Department of Physics, University of Manchester Institute of Science and Technology, P.O. Box 88, Manchester, M60 1QD, United Kingdom. Email: aaz@iapetus.phy.umist.ac.uk
[4] Space Telescope European Co-ordinating Facility, European Southern Observatory, Karl-Schwarzschild Strasse 2, D-85748 Garching bei München, Germany. E-mail: jwalsh@eso.org

Abstract. Radio continuum observations at 1.4, 4.8 and 8.6 GHz of the two Planetary Nebulae (PNe) in the Sagittarius dwarf galaxy reveal the elongated shape of Wray 16-423 and the extreme compactness of He 2-436. It is confirmed that He 2-436 is subject to local dust extinction.

Photoionization models for both PNe are obtained from two different codes, allowing theoretical uncertainties to be assessed. Wray 16-423, excited by a star of effective temperature 1.07×10^5K, is an ellipsoidal, matter-bounded nebula, except for a denser sector of solid angle 15%. He 2-436, excited by a 7×10^4K star, includes two radiation-bounded shells, with the very dense, low-mass, incomplete, inner shell possibly corresponding to a transitory event. The continuum jump at the He$^+$ limit ($\lambda 22.8$nm) agrees with NLTE model stellar atmospheres, despite the Wolf-Rayet nature of the stars. Both stars are on the same (H-burning) evolutionary track of initial mass (1.2 ± 0.1) $M_\odot$ and may be twins, with the PN ejection of Wray 16-423 having occured $\sim$ 1500 years before He 2-436.

The PN abundances re-inforce the common origin of the parent stars, indicating almost identical depletions with respect to solar for O, Ne, Mg, S, Cl, Ar, and K $(-0.55 \pm 0.07$ dex), and strong overabundances for carbon, particularly in He 2-436. He I lines consistently point to large identical overabundances for helium in both PNe. An excess nitrogen makes Wray 16-423 nearly a Type I PN.

These PNe provide a means to calibrate both metallicity and age of the stellar population of Sagittarius. They confirm that the youngest, most metal-rich population has an age of 5Gyr and a metallicity of [Fe/H]$= -0.55$, in agreement with the slope of the red giant branch.

Key words: Stars: AGB and post-AGB - (ISM:) planetary nebulae: general - (ISM:) planetary nebulae: individual: He 2-436 and Wray 16-423 - Galaxies: dwarf - Galaxies: individual: Sagittarius

arXiv:astro-ph/0009054 v1 5 Sep 2000

1. Introduction

Zijlstra & Walsh (1996) discovered that two previously catalogued Planetary Nebulae (PNe) belonged to the newly recognized Sagittarius dwarf galaxy (Ibata et al. 1994, 1995). In the course of a radial velocity survey (Zijlstra et al. 1997), He 2-436 and Wray 16-423 were found to coincide in both position and velocity with this galaxy. Optical spectroscopy for both objects (Walsh et al. 1997, hereafter Paper I), showed a $\sim$ –0.5dex depletion of N, O, Ne with respect to Galactic PNe (Kingsburgh & Barlow 1994), confirming that they were members of Sagittarius. Wolf-Rayet ([WR]) features were detected in both spectra.

Given that these objects are the closest extragalactic PNe ever identified [distance to Sagittarius is taken as 25kpc (Ibata et al. 1995), although Mateo (1998) gives 24kpc] and belong to a stellar system with a star formation history different from that of the Milky Way, it was decided to obtain radio continuum data and to improve on the abundances and other physical quantities of the nebulae and central stars by means of photoionization models.

2. Radio observations

2.1. Wray 16-423

Wray 16-423 was observed with the Australian Telescope Compact Array on 1997, June 19th, simultaneously at 8.6 and 4.8 GHz over a 12-hour integration. The array was in its '6A' configuration with baselines ranging from 330m to 5940m, maximizing the angular resolution. The radio source $1933-400$ was used for phase calibration. The amplitude calibration was based on $1934-638$, adopting the new fluxes of 5.826 Jy and 2.814 Jy at 4.8 GHz and 8.64 GHz respectively. (The new scale differs from the previous one, changing the spectral index between 3 and 6 cm

by 0.3. This scale agrees with the one used in the Northern hemisphere to within 1–2%.)

The data were analyzed using the Miriad and AIPS packages. A full calibration of instrumental polarization was done to optimize the flux calibration. Tests done during the observations showed a pointing accuracy of better than $10''$. Altitude-dependent pointing errors were minimized as the phase calibration was close to the target source. The calibrated data were Fourier transformed to produce images and cleaned to replace the 'dirty' point spread function by a Gaussian beam. A signal-to-noise ratio of 300 was measured before self-calibration, confirming the quality of the data.

The FWHM of the resulting Gaussian beam was $3.0'' \times 1.8''$ at 6 cm and $1.7'' \times 1.0''$ at 3 cm, with position angle near zero degrees, owing to the 12-hour integration. Because the point-spread function is mathematically known, sizes can be obtained even for sources several times smaller than the beam for sufficiently high signal-to-noise. Wray 16-423 was found to be slightly resolved at 3 cm, with equivalent FWHM of a Gaussian source of $0.6'' \times 0.3''$ at position angle 58 degrees (measured from North to East on the sky). At 6 cm a size of $0.85'' \times 0.3''$ was found with the same position angle. The PN appears unresolved along its short axis but the observed elongation is not an instrumental artefact, given that the position angle is quite different from that of the beam. Thus, Wray 16-423 may have an elliptical or otherwise elongated morphology with axial ratio of order 2:1 or more. Correction factors between FWHM Gaussian diameters and uniform disk diameters for slightly resolved sources are provided by Bedding & Zijlstra (1994) and van Hoof (2000): for Wray 16-423 the Gaussian diameter should be multiplied by a factor of 1.6, giving approximately $1''$ for the major axis. In Paper I, a ground-based [O III] image of Wray 16-423 was deconvolved and a $1.2 \times 0.8''$ ellipse with position angle 50° was found. The radio and optical descriptions are therefore in agreement within uncertainties.

The total flux of Wray 16-423 was 4.72 mJy at 6 cm and 4.31 mJy at 3 cm. The flux accuracy, limited by the noise in the map (0.06 mJy/beam) and the systematic uncertainty in the flux scale, is 0.20 mJy at the 3-σ level. The spectral index is found to be -0.08, very close to the theoretical value of -0.1 for optically thin radio emission, thus confirming the accuracy of the relative flux calibration.

2.2. He 2-436

He 2-436 was observed at the VLA on October 1, 1998, using 15-minute snapshots at 3.6 cm (8.4 GHz), 6 cm (4.89 GHz) and 20 cm (1.46 GHz). The array was in the 'B' configuration. 3C286 was used as flux calibrator and 1924-292 the phase calibrator. Due to the short integrations, the calibration is less accurate than for Wray 16-423.

After cleaning and self-calibration, He 2-436 was detected at all bands although very faint at 20 cm. The flux was determined as 0.6 ± 0.2 mJy at 20 cm, 3.9 ± 0.2 mJy at 6 cm and 4.9 ± 0.2 mJy at 3.6 cm. The uncertainty comes from the noise in the map (around 0.1 mJy/beam but 0.16 mJy/beam at 20 cm) and an estimate of the uncertainty in the flux calibration. The source was unresolved. At 3.6 cm where the beam was $2'' \times 0.8''$ (elongated NS), an upper limit to the size of $0.2''$ in the EW direction was found.

The turn-over frequency between optically thick and optically thin emission may occur near 8 GHz, suggestive of a high density PN. Assuming $T_b = T_e$ at 20 cm, the observed flux of 0.62 mJy corresponds to a source diameter of $0.12''$. The diameter may be larger if the optical depth is not constant across the nebula. The spectral index between 6 and 20 cm is -0.7, compatible with an r^{-2} density distribution. The interpretation may not be unique but a density gradient is detected in He2-436.

The radio position of He 2-436 is RA $19^h32^m06.72^s$, DEC $-34°12'57.3''$ (J2000), in agreement with the optical position given by Walsh et al. (1997). This differs from the J2000 listed position in the Strasbourg-ESO catalogue of Galactic PNe (Acker et al. 1992) but agrees with the star position in the finding chart.

3. Photoionization models

3.1. Computations

3.1.1. The codes

Models for these PNe were obtained from two photoionization codes which differed in their numerical methods and approximations: on the one hand, the code developed by J. P. Harrington (Harrington et al. 1982), as further modified by R. E. S. Clegg (Clegg et al. 1987) – hereafter the HC code – and updated for some atomic data according to the package developed by Shaw & Dufour (1995); on the other hand, the NEBU code, a descendent of the code of G. Stasinska, S. M. Viegas-Aldrovandi and D. Péquignot, as further developed by Péquignot (Petitjean et al. 1990; Morisset & Péquignot 1996). An overview of the characteristics of these and other codes is presented in Ferland et al. (1995).

Atomic data, notably from the IRON project, are reviewed by Storey (1997). More recent references of interest are Ramsbottom et al. (1997, 1999) for [Ar IV] and [Cl III]. The total recombination coefficients have now been reassessed for C, N and O (Nahar & Pradhan 1997; Nahar 1999), but are not yet known for some of the S, Cl, and Ar ions (e.g., Nahar 1995). In NEBU, a few coefficients were empirically calibrated from a new unpublished model of the PN NGC 7027: the $S^{2+} \rightarrow S^+$ and $Ar^{3+} \rightarrow Ar^{2+}$ total recombination coefficients were increased by factors 1.7 and 5 respectively. Note that, for $S^{3+} \rightarrow S^{2+}$, Nahar (1995) obtained a factor 5 increase.

3.1.2. Primary continua

In the HC computation, the central star energy distribution was taken from the NLTE model atmospheres of Clegg & Middlemass (1987). Given the luminosity L_* and the effective temperature T_{eff}, the surface gravity g was bound to give a stellar mass in the range $0.55 - 0.65\ M_\odot$, encompassing 80% of the PN nuclei (Stasinska et al. 1997).

However concerns may be expressed about standard stellar atmosphere models, particularly when applied to [WR] stars (*e.g.*, Kudritzki & Méndez 1993). m_V In the NEBU computation, the primary radiation was given a black-body shape (defined by L_B, T_B, equivalent to L_*, T_{eff}), except that the flux shortward of $\lambda 22.8$nm could be multiplied by an arbitrary factor f_4. This freedom allowed some consequences of varying the hardness of the ionizing continuum to be studied. Longward of $\lambda 22.8$ the black-body flux matches the model-atmosphere flux of a star with $T_{eff} = T_B - 1.5 \times 10^4$K and mass $0.6\ M_\odot$, appropriate for a $M = 1.2\ M_\odot$ parent star with $Z = 0.004$ (Sect. 4.6). This relation will be used to convert T_B's into T_{eff}'s.

3.1.3. Gas distributions

Both computations were done in spherical symmetry, with filling factor unity and uniform elemental abundances. Departure from spherical symmetry was approximately taken into account by combining two spherical cases (two-sector models). In the HC computation, the density was constant, sometimes constant by steps (with linear transitions), throughout the nebula. In the NEBU computation, the gas pressure was constant, particularly in the vicinity of the ionization fronts, or constant by steps with analytically smooth transitions. No attempt was made to model the effect of the dust possibly mixed with the ionized gas.

3.2. Observations

3.2.1. Optical data

A considerable asset of remote PNe from the standpoint of photoionization modeling is that their small apparent size allows global spectra to be secured. Optical line fluxes were taken from Paper I. In col. 6 of Table 2 and col. 4 of Table 4 below, the 1-σ errors are from the Gaussian fits to the lines and do not include possible systematic errors. In Wray 16-423, the Hβ flux was corrected for He II.

Concerning blends, [Ar IV] 471.3nm was corrected for He I 471.1nm ($\sim 34\%$ and 85% of the blend in Wray 16-423 and He 2-436 respectively, see below and Sect. 4.3), [S II] 406.9nm for C III+O II ($2.87 \times I_{\lambda 418.7} + 0.518 \times I_{\lambda 465.1}$, typically 23% and 15% in Wray 16-423 and He 2-436 resp.), and [S II] 407.6 for C II+O II ($0.074 \times I_{\lambda 426.7} + 0.349 \times I_{\lambda 465.1}$, typically 18% and 14% resp.) (see Péquignot et al. 1991; Storey 1994; Liu et al. 1995; Davey et al. 2000). These corrections were applied consistently for each model. Thus the computed C II 426.7nm flux, rather than the observed

one, was used, considering the large observational uncertainty. (The fluxes of [O II] 732.0nm and 733.0nm should be exchanged in Table 4 and Table 5 of Paper I; only the sum of this multiplet is used for diagnostics. In Table 4 of Paper I, the $\lambda 471.1$ flux should read 1.40, not 1.49).

In Wray 16-423, after correcting for [S III] 372.2nm, the flux quoted for H I 372.2nm (B14) is still significantly larger than the theoretical one, whereas all other Balmer lines from B9 to B19 agree with theory (Storey & Hummer 1995) within uncertainties (B16 is too strong, but blended with He I, Sect. 4.3). No other blend with B14 is known but the line is close to [O II] 372.6nm and the excess flux of B14 was attributed to [O II] (with enhanced uncertainty). A similar excess, present in He 2-436, was treated in the same manner, but the correction to [O II] is tentative owing to the poorer definition of the continuum level. In these PNe, the [O II] doublet ratio is little sensitive to physical conditions. These corrections to $\lambda 372.6$ lead to new observed ratios in better agreement with theory.

The asymmetrical feature $\lambda 723.6$ (noted [Ar IV] in Paper I) is dominated by C II(3) $723.1+3.6+3.7$nm, whose strength is 1.04 times that of $\lambda 426.7$ in Case B and small in Case A (Davey et al. 2000). Moderate and "moderately small" departures from Case B are expected for Wray 16-423 and He 2-436 respectively. Indeed, after removing [Ar IV] 723.7nm (below), the ratio $I_{\lambda 723.6}/I_{\lambda 426.7}$ is 0.58 and ~ 0.82 in Wray 16-423 and He 2-436 respectively. Removing C II 658.0nm from [N II] 658.3nm, assuming half Case B, leads to an improved [N II]-doublet ratio.

For densities of interest, the sum of the red [Ar IV] multiplet is 3.3 times the intensity of [Ar IV] 726.3nm (Mendoza & Zeippen 1982), detected in Wray 16-423 at low signal to noise. In He 2-436, [Ar IV] 726.3nm and 717.1nm, of similar intensities, were not detected: a 3-σ upper limit to the multiplet was taken as 3 times the 2-σ limits.

The observed [Ar III] ratio $I_{\lambda 713.6}/I_{\lambda 775.1}$ is ~ 5.3 in both objects (Paper I) and the theoretical value is 4.15 (Mendoza 1983). The adopted sum for the multiplet was based on $\lambda 713.6$, using a doublet ratio intermediate between the observed and theoretical values and increasing the error bar. In He 2-436, the "2-σ detections" of the [Cl III] lines (Paper I) were replaced by 3-σ upper limits.

3.2.2. Dust extinction and absolute Hβ fluxes

The radio fluxes for Wray 16-423 lead to log $I_\beta = -11.89 \pm 0.02$ and the observed log $F(H\beta) = -12.09 \pm 0.03$ implies an extinction $c_{radio} = 0.20 \pm 0.04$, which compares very well with the extinction derived from the Balmer decrement, $c_{Balmer} = 0.20 \pm 0.04$ (Paper I). Considering this excellent agreement and the accuracy of the radio fluxes, the uncertainty inherent to the reddening correction should be negligible and the de-reddened absolute Hβ flux be determined to better than 0.03dex.

The shape of the radio continuum of He 2-436 indicates that the fully optically thin regime may occur

above 8 GHz, the highest frequency available. A simple extrapolation suggests an optically thin flux ≈ 5.4 mJy, which, in combination with $F(H\beta)$, would lead to $c_{radio} = 0.50\pm0.07$, smaller than $c_{Balmer} = 0.61\pm0.05$. The interpretation of the Balmer decrement may be affected by extinction internal to the H^+ region and, particularly, by local uneven absorption due to a neutral envelope, as in the case of NGC 7027 (*e.g.*, Robberto et al. 1993) since the ionized mass of He 2-436 is small. Now, in case of uneven dust extinction, the Balmer-decrement method *underestimates* the true average extinction, at variance with what observational data suggest. Thus, until radio fluxes are obtained at higher frequencies, the Balmer-decrement reddening is adopted on account of the excellent agreement between c_{radio} and c_{Balmer} in the case of Wray 16-423.

In fact it is anticipated that the model results (Sect. 3.4, Table 4) will indicate that, assuming $c = 0.61$, the de-reddened $H\alpha/H\beta$ of Paper I is off by 2% for He 2-436, hence a new best reddening correction with reduced error bar $c_{Balmer} = 0.58 \pm 0.03$, still compatible with the value of Paper I but somewhat closer to c_{radio}. In the following, this new c_{Balmer} will be used to obtain de-reddened optical fluxes relative to $H\beta$. The present high-frequency radio fluxes are not too much affected by self-absorption and are more accurate than the $H\beta$ flux, taken in this case from Webster (1983): most of the uncertainty on c_{radio} and thus presumably most of the difference between c_{radio} and the new c_{Balmer} arise from the uncertainty of 15% on $H\beta$, not from the extrapolation of the radio fluxes to optically thin frequencies. It can therefore be suspected – as models will confirm – that the best estimate for the $H\beta$ flux corresponds to the lower end of the interval allowed by the error bars, namely Webster's flux divided by 1.15.

3.3. Wray 16-423

3.3.1. HC computation

Wray 16-423 is still a rather dense and young PN and it is relatively safe to assume that nebular material is present along any direction from the star. The total covering factors will be taken equal to unity.

The one-component constant-density model is described in col. 2 of Table 1 and the line intensities are given in col. 2 of Table 2 ("Thin"). The outer radius of this model roughly corresponds to the observed mean apparent diameter of $1.0''$. This "thin" model (optical depth $\tau_{13.6} = 7$ at 13.6 eV) is a poor fit to low-ionization line fluxes.

Consideration was given to an optically thick component obtained by increasing the outer radius from 0.062 to 0.073 pc. On its own, this "thick" model (col. 3 of Table 2) does not reproduce the observations. Wray 16-423 cannot be spherically symmetric: if the optical depth is large enough to account for [O I], then [O II] is too large.

Table 1. Models for Wray 16-423

Model	HC	NEBU
Distance/kpc	25	25
$(T_{eff}$ or $T_B)/10^3$K	90	125
$(L_*$ or $L_B)/10^3 L_\odot$	4.60	5.04[a]
log g (f_4)	5.3	(0.31)
$N_{13.6}/10^{47}$s^{-1}	3.11	2.95
Filling factor	1.0	1.0
Mass/$10^{-2} M_\odot$	18.8	24.8
Radius/10^{-3}pc:		
(Thin sector)	33 - 62	23 - 80
(Thick sector)	33 - 73	23 - 51
$N_H/10^4$cm^{-3} (and covering factor):		
(Thin)	0.60 (0.90)	0.36 (0.83)
(Thick)	0.60 (0.10)	0.95 (0.17)
Gas pressure/10^{-8}CGS:		
(Thin)	-	1.4
(Thick)	-	3.5
$\tau_{13.6}$(Thin)	7.0	6.7
Abundances by number:		
H	1.00	1.00
He	0.107	0.107[b]
C $(\times10^5)$	67.6	73.7
N $(\times10^5)$	5.79	4.60
O $(\times10^5)$	20.4	21.4
Ne $(\times10^5)$	3.33	3.59
Mg $(\times10^5)$	-	0.95
S $(\times10^5)$	0.61	0.440
Cl $(\times10^5)$	-	0.0077
Ar $(\times10^5)$	-	0.090
K $(\times10^5)$	-	0.0045

[a] 4.22, correcting for f_4 (see Sect. 3.3.3).
[b] Adopted He abundance will be 0.108 (Sect. 4.3).

A composite of the thin and thick cases (Table 2, col. 4), accounting for the [O II] lines, is an improvement in that not only [O II], but [S II] and [O I] as well are now better matched, although [O I] is still underestimated. C II 426.7nm appears underestimated by 30%, still within the 1-σ error bar: this result should be considered a success of this model since carbon is determined by the global energy budget, whereas T_{eff} is constrained by the [O III] ratio. The [S II] line ratios are now not as closely matched as in the previous "thin case", suggesting that low-ionization lines are not produced at a unique density.

3.3.2. NEBU computation

The low-ionization line fluxes were improved by introducing a thick sector in the HC model. Nonetheless, assuming a constant density throughout the nebula, the radiation-bounded sector was left as the long axis. In elongated Galactic PNe, the short axis generally corresponds to the dense, optically thicker "equator".

The NEBU model (col. 3 of Table 1 and col. 7-9 of Table 2) consists of two constant-pressure sectors, im-

plying five free parameters: two gas pressures, one optical depth, one covering factor and the inner radius. The matter-bounded and radiation-bounded sectors now have angular "diameters" $1.31''$ and $0.84''$ respectively, in fair agreement with observation.

In col. 10 of Table 2 are given the ratios of computed to observed fluxes for all lines (and the 1-σ observational uncertainties). Very few of these ratios are significantly different from unity.

The two-sector description is successful for all [N II], [O II], [S II], and [Cl III] lines, once a larger density, called for independently by geometrical information, is postulated for the short axis. The [Ar IV] doublet ratio suggests an even denser region which may be accomodated with [N II] and [S II] ratios within uncertainties, but proved difficult to reconcile with the [O II] ratio in this description.

The [O I] doublet is now predicted at $\sim 60\%$ of the observation, which can be considered satisfactory. Departure from strict ionization/thermal equilibrium, quite possible in ionization fronts, may increase the [O I] emission.

A 50% mismatch of the argon ionization balance is left as a noticeable imperfection of the model. Atomic data, notably the di-electronic recombination rates introduced on empirical grounds (Sect. 3.1.1), may be incorrect for argon and this discrepancy does not justify considering a more elaborate gas distribution. Nonetheless, if part of the high-ionization region is denser than the constant-pressure dense sector, both the [Ar IV] doublet ratio and the [Ar IV] to [Ar III] ratio can improve without much influencing the [O II] ratio. This possibility was not explored.

3.3.3. Comments

In the NEBU model, the "colour temperature" of the central star below the He$^+$ ionization limit is $T_B = 1.25 \times 10^5$K. Subtracting 1.5×10^4K from T_B (Sect. 3.1.2), the $T_{\rm eff}$ of the model star derived from the NEBU calculation exceeds the one used in the HC calculation by 2×10^4K. A much lower T_B (and correspondingly larger f_4) results in a weaker, still acceptable C II (reminiscent of the HC result) but the [S II] line fluxes can no longer be reproduced in the NEBU computation to the quoted accuracy. Good results are obtained in the range $[T_B = (1.20 - 1.35) \times 10^5$K, $f_4 = (0.342 - 0.253)]$ although the upper bound to T_B is loosely defined due to the asymptotic behaviour of intensity predictions, while the lower bound is not strict either considering uncertainties in some atomic data for sulfur.

A major feature of model atmospheres of hot PN nuclei is the amplitude of the He$^+$ ionization-limit discontinuity at $\lambda 22.8$. The discontinuity factor, as derived empirically from NEBU models of Wray, decreases from $f_4 = 0.406$ for $T_{\rm eff} = 1.0 \times 10^5$K ($T_B = 1.15 \times 10^5$K) to $f_4 = 0.309$ for $T_{\rm eff} = 1.1 \times 10^5$K ($T_B = 1.25 \times 10^5$K, present model), while the same quantity increases from 0.36 to 0.50 according to the standard NLTE stellar atmosphere models of Clegg &

Middlemass (1987) (assuming a star mass of 0.6 $M_\odot$, but the dependence on g is moderate here). These determinations intersect for $T_{\rm eff} = 1.02 \times 10^5$K, near to the lower end of the $T_{\rm eff}$ range leading to the most satisfactory NEBU models. Thus the Clegg & Middlemass (1987) results appear to provide a fair representation of the actual spectral energy distribution of the nucleus of Wray 16-423 as depicted from nebula properties. It is frequently suspected that, in order to best account for nebular properties, the departure from a black-body distribution in the EUV continuum of hot stars should be *less* than in standard NLTE model atmospheres (*e.g.*, Harrington 1989). Also detailed radiation-transfer calculations with self-consistent treatment of wind in hydrodynamic NLTE model atmospheres show a significant rise in the continuum flux shortwards of $\lambda 22.8$, thus partly "erasing" the discontinuity (Kudritzki & Méndez 1993; Yamamoto et al. 1997). Finally, shocks may develop in the strong winds of hot [WR] stars and produce extra emission (*e.g.*, Feldmeier et al. 1997). In this context, the *relatively large He$^+$ discontinuity* found to characterize the nucleus of Wray 16-423 might be due to the large helium abundance in its atmosphere.

Considering that, for large $T_{\rm eff}$'s, (1) the "asymptotic" behaviour of the NEBU solutions becomes artificial and (2) a large $\lambda 22.8$ discontinuity is then unlikely whatever the helium content of the atmosphere may be, the lower end of the NEBU $T_{\rm eff}$ range must be preferred. One more aspect is the shape of the nebula: for large $T_{\rm eff}$'s, the model nebula is found to become spherical and bigger than observed. The final best estimate, which takes into account uncertainties on [S II] atomic data as well as the tendency shown by the HC model, is:

$T_{\rm eff}$(Wray 16-423) = $(1.07 \pm 0.10) \times 10^5$K.

The source luminosity in the NEBU model is 92% of that of the HC model star. The number of ionizing photons $N_{13.6}$ differs by $\sim 5\%$ (Table 1). Part of this difference can be ascribed to the slight overestimate of I_β in the HC model (+3.6% on average for I_β and radio, col. 4 of Table 2). Moreover, the black bodies used in the NEBU computation are intended to represent the ionization radiation shortward of 91.2nm, whereas the stellar flux is generally larger longward owing to the H^0 discontinuity: for high $T_{\rm eff}$'s the correction to L_B from this cause is a few percent. Thus, despite the different nebula structures considered, both models lead to almost identical central star luminosities. The adopted luminosity is:

L_*(Wray 16-423) = $(4.35 \pm 0.15) \times 10^3 L_\odot$,

where the 3% uncertainty from modeling is to be added to the 4% observational uncertainty on I_β.

3.4. He 2-436

3.4.1. HC computation

The ionized mass of He 2-436 is small and it is likely to be radiation bounded in all directions. Using the oxygen

abundance of Paper I, the [O III] ratio could be matched by taking $N_H = 1.3 \times 10^5 \text{cm}^{-3}$ in the O^{2+} zone, but the [O II] 372.7nm/732.5nm ratio indicates a lower density. An outer shell was therefore added to the main shell. The model (col. 2 of Table 3 and results in col. 2 of Table 4) meets difficulties in reproducing the strengths of [O II] and [O I].

The model is optically thick at 1.5 and 4.9 GHz and the predicted fluxes agree very well with the observed fluxes at these frequencies. Even though the model is not yet completely thin at 8.4 GHz, it appears to overestimate the flux there, confirming the suspicion that F_β has been overestimated (Sect. 3.2.2).

The HC model helium abundance exceeds the empirical one. Standard empirical collisional contributions to He I lines are larger than in this model, which allows for the photoionization of 2^3S (Clegg & Harrington 1987). This large helium abundance may be spurious, considering the bad fit to the He I lines. Photoionization of 2^3S may be partly inhibited by dust absorption (Sect. 4.3).

3.4.2. NEBU computation

The gas distribution adopted in the HC computation cannot account for low-ionization lines. The importance of the low-ionization region is controlled by $N_{13.6}/(r^2 \times N_H)$. $N_{13.6}$ is determined by I_β, N_H by low-ionization line diagnostics, and the size r of the emission region by the 20 cm continuum surface brightness. Increasing low-ionization line fluxes in the *strictly spherical* model implies that part of the photoionized gas, not dominant in terms of Hβ emission, lies further away from the star than the bulk of emitting material. The radio-continuum slope suggests a geometrically thick nebula with density gradient (Sect. 2.2).

The NEBU spherical model consists of two narrow shells, separated by a low-pressure region of substantial mass but negligible emission. The parameters describing the structure are the pressure and radius of each shell, and the fraction of I_β emitted by the outer shell. There are thus five structure parameters as in the computation for Wray 16-423. Models could be found which matched most line fluxes as closely as in the case of Wray 16-423 with the exception of the [N II] lines: the flux ratio [N II] 658.4+4.8nm/575.5nm was systematically predicted too large by 40–50%, a discrepancy much larger than the 10% observational uncertainty. An example is provided by Model M1 (Table 3, col. 3). Flux predictions for M1 are not given in Table 4, as they turn out to almost coincide with those of Model M2 below, except for the [N II] lines and the radio fluxes. The [O II] and [N II] lines cannot be made compatible in Model M1 because their ratios point to significantly different average densities. A combination of regions of similar ionization but greatly different densities is required. Hence low-ionization regions must exist at different distances from the star, indicating a failure of the assumption of spherical symmetry. Aside from this spectroscopic verdict, the structure obtained assuming strict

sphericity is artificial in that the inner shell absorbs most of the photons: a moderately larger column density would suffice to exhaust the ionizing radiation. An inner shell, thick along some directions and thin along other ones, is more realistic. Another difficulty with spherical models is that the shells must be totally disconnected from each other: absorption by low-density gas in between the shells would produce high-ionization lines and reduce the amount of radiation available in low-ionization regions.

Two-sector radiation-bounded models were built, with only four parameters describing the gas distribution: two pressures, one covering factor and the inner radius. In accordance with Sect. 3.2.2, the absolute Hβ flux is taken as only 87% of the flux quoted by Webster (1983). Despite reduced freedom, the two-sector model (Model M2: col. 4 of Table 3 and cols. 5-7 of Table 4) is more successful than any spherically symmetric model.

Nonetheless the low-frequency radio flux (1.5 GHz) is discrepant. The total radial optical depth at 1.5 GHz is large (~ 8), but the outer "radius" of the low-density sector (radial optical depth ~ 1) is also large in order to account for the strength of those low-ionization lines easily quenched by collisions. Now, radio fluxes given in col. 7 of Table 4 are rather *upper limits* as they result from simply

Table 3. Models for He 2-436

Model	HC	M1	M2
Distance/kpc	25	25	25
$(T_{\text{eff}}$ or $T_B)/10^3$K	70	80	85
$(L_*$ or $L_B)/10^3 L_\odot$	6.90	5.06^a	5.12^b
log g $\quad (f_4)$	4.7	(.10)	(.08)
$N_{13.6}/10^{47}\text{s}^{-1}$	4.82	3.76	3.76
Filling factor	1.0	1.0	1.0
Mass/$10^{-2} M_\odot$	1.9	2.0	3.8
Radius/10^{-3}pc:			
(Inner shell)	5.3-9.5	7.3-8.4	8.3-9.0
(Outer shell)	9.5-11.0	18.4-19.3	8.3-31.
$N_H/10^4\text{cm}^{-3}$ (and covering factor):			
(Inner)	13.	22.	27. (.62)
(Outer)	6.0	6.4	2.0 (.38)
Gas pressure/10^{-8}CGS:			
(Inner)	-	75.	85.
(Outer)	-	23.	7.
Abundances by number:^{c}			
H	1.00	1.00	1.00
He	0.12	0.104^d	0.104^d
C $(\times 10^5)$	150.	110.	111.
N $(\times 10^5)$	3.50	2.34	2.64
O $(\times 10^5)$	21.0	24.5	23.1
Ne $(\times 10^5)$	3.16	3.54	3.42
S $(\times 10^5)$	0.50	0.419	0.391
Ar $(\times 10^5)$	–	0.060	0.060

^{a} 4.82, correcting for f_4 (see text).
^{b} 4.85, correcting for f_4 (see text).
^{c} Mg, Cl and K as in Wray 16-423 (Table 1).
^{d} Adopted He abundance will be 0.108 (Sect. 4.3).

averaging the individual fluxes, that is without considering possible "shielding" effects between sectors. Given that self-absorption is important and spherical symmetry is abandoned, geometry must be considered. The nebula may, for example, be elongated in the direction of the observer, then reducing somewhat the 1.5 GHz flux. A larger reduction would obtain if a smaller solid angle were given to the low-density sector but some lines would then not be nearly as well matched as in Model M2. At this stage it is worthwile to note that (1) this two-sector model is a coarse representation and (2) some atomic data for ionization equilibria used in judging the model fit (*e.g.*, sulfur) are not of ultimate accuracy. Density may be larger in part of the inner layers of the otherwise "low-density" sector, then reducing the outer radius and the 1.5 GHz flux.

The high-frequency radio fluxes (4.9 and 8.4 GHz) are 10–20% too large in Model M2, but the radio continuum slope is matched, suggesting that I_β may be even less than the lower limit of the error bar. However, aspect effects in the incomplete inner shell introduce some uncertainty in the computed flux: the 8.4 GHz optical depth across this component is only 0.19 radially, but 0.85 near to the edge. The uncertainty of geometrical origin amounts to $\sim 10\%$ and Model M2 can be considered as compatible with both the optical and high-frequency radio fluxes within errors.

As for the fit to the optical spectrum (relative to Hβ), Model M2 for He 2-436 is as satisfying as model M for Wray 16-423 and the two discrepancies left in M2 are very reminiscent of those already noted in the case of Wray 16-423, namely M2/O = 0.58±0.01 compared to M/O = 0.56±0.02 for [O I] 630.0+6.3nm and 1.9±0.4 compared to 1.6±0.1 for the ratio [Ar IV]471.1+4.0/[Ar III]713.6+775.1.

3.4.3. Comments

Due to observation uncertainties ([O II] 372.7, [S II] 406.9, C II 426.7, [Ar IV] 471.1) and partial collisional quenching of [O III], a range of two-sector NEBU models, in which all parameters were coherently fine-tuned, could be obtained. Model M2 is typical. After correcting for f_4, the fluctuation of black-body luminosity L_B among the NEBU models is $\sim 1\%$ and L_B is ~ 1.42 times less than L_* (HC model). The ionizing-photon output $N_{13.6}$ is 1.28 times less than in the HC model. The differences between the HC and NEBU results can be understood as follows.

Note first that the most significant radio flux in terms of photon counting, namely the 8.4 GHz flux, is predicted by the HC model as 1.25±0.05 times the observed value. Reaching agreement would require lowering $N_{13.6}$ by a factor over 1.3, as the radio optical depth decreases together with the column density of ionized material. The HC model corresponds to the original dereddened flux I_β(c=0.61), the NEBU model to 0.87×I_β(c=0.58), hence a factor 1.20 smaller. The remaining factor 1.28/1.20 = 1.06 on $N_{13.6}$ corresponds to the larger fraction of photons re-

moved from the ionizing field by He^0 photoionisation in the HC model, due mainly to the larger helium abundance.

The same factor 1.28 applies to L_*(HC), but a supplementary factor arises from the fact that model stellar atmospheres for $T_{\mathrm{eff}} \sim 7 \times 10^4$K show quite a large discontinuity at 1 Ryd, implying an upward correction to L_B. After removing the effects of considering different photoionization rates for He(2^3S) and black bodies instead of star atmospheres, the differences between the HC and NEBU central star luminosities essentially reflect a different emphasis on which absolute flux should be favoured. Favouring the more accurate 8.4 GHz flux, while respecting the error bars on I_β, is taken as the best option. In conclusion, the best estimate for L_* is the value obtained in the HC computation, divided by 1.28, that is:

L_*(He 2-436) = $(5.40\pm0.40)\times10^3 L_\odot$,

where the 7% uncertainty is from models only, to be added to the 7% observational uncertainty on the high-frequency radio continuum fluxes. The model uncertainty on L_* is substantial, considering that the connection between L_* and the ionizing flux is not straightforward and that, due to the dependence on geometry, even a fully accurate 8.4 GHz flux does not imply a unique value for L_* (Sect. 3.4.2).

If the luminosity of the central star of He 2-436 is not very accurately determined from models and high-frequency radio data, the effective temperature seems to be. The most satisfactory NEBU models indicate $T_B = (0.85\pm0.05)\times10^5$K, which converts (Sect. 3.1.2) into:

T_{eff} = $(0.70\pm0.05)\times10^5$K,

in agreement with the HC result (Table 3, col. 2).

Some freedom on star parameters is currently unavoidable, given the presence of quite prominent Wolf-Rayet features in the spectrum of He 2-436 and the questionable accuracy of stellar atmosphere models for this class of stars (*e.g.*, Crowther et al. 1999). If the λ22.8 discontinuity is large, perhaps as a consequence of the large helium abundance in the atmosphere, relatively high T_{eff}'s are possible. If, on the other hand, this discontinuity is "erased" by the emission of a strong hot wind, then relatively low T_{eff}'s may have to be preferred. Considering these additional uncertainties, our estimate for the He 2-436 star effective temperature is, more conservatively:

T_{eff}(He 2-436) = $(0.70\pm0.10)\times10^5$K.

A more definite picture should await more accurate fluxes for some optical lines (see above) and new spectroscopic diagnostics. The He 2-436 models may be distinguished thanks to their UV lines (Table 4). In models with relatively cool central stars, the carbon lines are weak. In other models, these lines are as strong as [O III].

4. Discussion

4.1. Appraisal of the models

The two codes used to model the two Sagittarius PNe reached agreement under similar assumptions, confirming

the reliability of the calculations. A few differences, notably on sulfur, were understood in terms of atomic data updating. The HC approach was restricted to simple assumptions and provided the basis for the more systematic approach adopted with NEBU. The HC and NEBU models led to similar properties for both the star and the chemical composition, but some significant differences demonstrated the influence of the adopted gas distribution. In the case of Wray 16-423, the 33 independent observables available (1 imagery; 3 photometry; 29 relative optical spectroscopy, out of which 18 and 11 are accurate to better than 4% and 2% respectively) against the 18 free parameters of the NEBU model (1 reddening; 10 abundances; 2 stellar; 5 nebular parameters) lead to some 15 "redundancies" to estimate the model consistency.

Correspondingly in He 2-436, 27 observables (4 photometry; 23 relative optical spectroscopy, out of which 12 and 8 are accurate to better than 4% and 2% respectively) against 14 parameters (1 reddening; 7 abundances; 2 stellar; 4 nebular parameters), give 13 redundancies.

Except for [Ar IV] and [O I], all spectroscopic features are explained to 1 σ by the NEBU models of both PNe. The discrepancies for either [Ar IV] or [O I] are strikingly similar in both objects (end Sect. 3.4.2), suggesting they have systematic origins. The mismatch to [O I] has no effect on the oxygen abundance determination.

The overestimation of the radio flux of He 2-436 may result from not taking into account the mutual shielding of the two sectors and possible aspect effects (Sect. 3.4.2).

In conclusion, physically independent lines from different elements and ions, involving redundant information, could be made to fit into self-consistent pictures. Although the model for He 2-436 is not really unique (Sect. 3.4.2) and the model for Wray 16-423 may be too coarse a description of the innermost regions (Sect. 3.3.2), these models appear as valuable descriptions of the Sagittarius PNe, giving a high degree of confidence in the accuracy of the derived elemental abundances and central star properties.

4.2. Geometry of Wray 16-423 and He 2-436

Both PNe were described in terms of two-sector models, but the geometrical interpretation must be different. The moderate contrasts in density and radius of the two sectors of Wray 16-423 suggest an ellipsoidal structure, also indicated by radio and optical imaging. The short axis is denser and radiation bounded as in many relatively young Galactic PNe. The large contrasts in density ($\sim$15) and thickness ($\sim$30) found for the sectors of the He 2-436 model suggest a two-shell geometry in which the outer shell is illuminated by radiation leaking through "holes" in a very dense radiation-bounded incomplete inner shell.

The ionized mass of the inner shell of He 2-436 is only $\sim 4 \times 10^{-3}$ $M_\odot$. This shell could correspond to a recent episode of mass ejection resulting from a late thermal pulse during the early post-AGB phase (*e.g.*, Schönberner

1997). With time, this shell may rapidly grow optically thin and be barely detectable if its total mass is small, then resembling the small amount of dense optically thin gas suggested by the [Ar IV] ratio in Wray 16-423.

The mass of He 2-436, obtained from the ionized gas and completing the outer shell assuming spherical symmetry, is about a third of the mass of Wray, consistent with He 2-436 being still radiation bounded in all directions. It will be argued in Sect. 4.7 that these PNe are quite similar objects, despite their very different appearance.

4.3. Helium abundance

A number of He I lines were observed in the Sagittarius PNe (Paper I), providing a way to check the consistency of the data sets used (theory and observation) and the reliability of the helium abundance determination.

In the NEBU models, all lines from levels $n < 6$ of He^0 are computed using recent effective recombination coefficients (Smits 1996; Smits, 1999, private communication) and collision strengths (Sawey & Berrington 1993) and accurate radiative transition probabilities (Kono & Hattori 1984). New fitting formulae are accurate to typically 0.2% (maximum error $\sim$ 1%, generally at a few 10^2 K). Case B recombination is assumed for all singlet lines but 2^3S $-n^3$P self-absorption is taken into account.

2^3S $-n^3$P self-absorption and fluorescence are treated in a semi-empirical local-escape formalism: the escape formula is taken as a guideline to connect the different probabilities (for the different transitions at the different locations in the nebula) and a constant velocity width is *chosen* to account for λ388.8 (2^3S -3^3P).

In col. 1 of Table 5 are given the wavelengths for 9 triplet and 8 singlet lines of He I. The observed dereddened intensities and upper limits ("O", Paper I with modified reddening correction for He 2-436, Sect. 3.2.2), the model intensities ("M", NEBU models, Table 2 and Table 4) and their ratios ("M/O", with one more exact digit) are given in cols. 2-4 and cols. 5-7 of Table 5 for Wray 16-423 and He 2-436 respectively (concerning col. 8, "M'/O", see below). Subtracted blends are noted in col. 9 ("Comments") of Table 5. 1-σ errors are attached to the M/O values.

In Table 5, the three strongest He I lines, predominantly excited by recombination and not much sensitive to departure from Case B or self-absorption ($\lambda\lambda$ 587.6, 447.1, 667.8), agree remarkably well with each other in both PNe. (λ667.8, accurately measured in He 2-436, is further considered below). Next λ402.6 and λ492.2 are fairly well explained, although λ402.6 would call for some extra excitation: this line is the strongest one from an $n = 5$ level and collisional excitation rates may not be accurate for $n > 4$ (Sawey & Berrington 1993).

λ471.3 was de-blended from [Ar IV] 471.1nm using the [Ar IV] doublet ratio from models (instead, in Tables 2 & 4, the theoretical He I 471.3nm from col. 3 & 6 of Table 5 was

subtracted from $\lambda 471.2$). The large M/O for $\lambda 471.3$nm in the case of Wray 16-423 (Table 5) is likely to arise from a problem with [Ar IV] (as assumed in Sect. 3.3.2). Indeed He I 471.3nm is correctly predicted in the case of He 2-436, where [Ar IV] 471.1nm contributes little to the blend: this is interesting as $\lambda 471.3$ is most enhanced by collisions. $\lambda 706.5$, mainly excited by collisions from 2^3S, is correctly predicted in He 2-436, but not in Wray 16-423, where the 2^3S population may therefore be incorrect.

Photoionization of 2^3S by the diffuse field is dominated by resonance lines (chiefly Lα), whose radiation density is sensitive to dust absorption (Clegg & Harrington 1987). The IRAS flux from He 2-436 is large, suggesting that the Lα radiation is substantially absorbed in this nebula. In standard NEBU models, the 2^3S photoionization by Lα was ignored. This should be a good approximation for Wray 16-423 but possibly not for He 2-436.

A new He 2-436 model similar to M2 (Sect. 3.4.2 and cols. 5-8 of Table 4), noted M2', was run assuming a uniform photoionization rate for 2^3S by the diffuse field. Clegg & Harrington (1987) note that the photoionization rate of 2^3S may not exceed 10-15% of the collisional destruction rate. In M2', the uniform photoionization rate amounts on average to $\sim$ 6% and 50% of the destruction rate for the dense and dilute sectors respectively: in this way part of the diffuse field produced in the incomplete inner shell is implicitly not processed locally but escapes into the outer shell where it adds to the weaker local diffuse field. The actual photoionization rates are not expected to be much larger than these values. In the new solution, the carbon abundance is 5% larger and the helium abundance increases from 0.1041 to 0.1072. The new ratios M'/O of predicted to observed He I line fluxes are given in col. 8 of Table 5. If $\lambda 706.5$ is now somewhat underestimated, the overall agreement turns out to be even better than in the standard case. The relative difference between $\lambda 667.8$ and $\lambda 587.6$ is decreased from 0.045±0.020 to 0.023±0.020. Thus the large photoionization rate for 2^3S, expected on general grounds in the conditions of He 2-436, is to some extent confirmed by the improved fit to observations.

Case A intensities (no 1^1S$-n^1$P photon degraded into non-resonant He I photons; Brockelhurst 1972) are given in comments of Table 5. Departure from Case B is likely for He I singlet lines as resonance photons are destroyed by H^0 photoionisation in the H$^+$ region or escape at the PN boundary. Indeed M/O is greater than unity for $\lambda 728.1$ in both PNe (Table 5). The departure from Case B appears larger in Wray 16-423, in qualitative agreement with the fact that this PN is less radiation bounded. Other lines sensitive to the Case B assumption are very weak and/or badly blended. $\lambda 501.5$, lost in the [O III] wing, is not listed. He I 396.5 is extracted from [Ne III]396.8 using the [Ne III] doublet ratio ([Ne III] is 95-98% of the blend) with the right order of magnitude: the $\lambda 396.5$nm flux (0.54±0.44 and 0.86±1.00 for Wray 16-423 and He 2-436 respectively)

loosely confirms a departure from Case B, with again a possibly larger effect in Wray 16-423 than in He 2-436.

The best helium abundance turns out to be 0.1076 by number in both PNe, with estimated uncertainties 1.5% and 2.5% for Wray 16-423 and He 2-436 respectively.

4.4. Abundances

In Table 6 are listed the empirical (cols. 2 & 4; Paper I) and model (cols. 3 & 5) abundances determined for the Sagittarius PNe. The model abundances are based on the abundances listed in Table 1 and Table 3, giving a larger weight to the NEBU abundances (Sect. 4.1). The errors on the abundances reflect the different model determinations and the range of acceptable solutions found in the course of the NEBU exploration (see also Péquignot et al. 2000). Larger errors were adopted for those abundances based on weak lines from only one ionic stage (Mg, Cl, K). The empirical He, C, O, Ne and Ar abundances of Paper I are generally confirmed. The sulfur abundance is increased in both PNe, especially in He 2-436. The nitrogen abundance is strongly increased in He 2-436, not in Wray 16-423.

The abundances are compared to a mean for non-Type I Galactic PNe (col. 6 of Table 6; Kingsburgh & Barlow 1994) and solar abundances. Since some of the ("preliminary") standard solar abundances listed by Grevesse & Sauval (1998) are marginally discordant from those generally taken for years as "standard" (Anders & Grevesse 1989) and the differences may be sufficient to influence the interpretation of the PN results, both sets of solar abundances are listed (col. 7 of Table 6) and the uncertainties attached to them are omitted, except in the case of sulfur for which the photospheric and meteoritic determinations were exchanged, keeping by chance the weighted mean unchanged. Columns $8-10$ of Table 6 provide the logarithmic differences between the model Sagittarius PN or empirical Galactic PN abundances on the one hand and the different solar abundances on the other hand.

The enrichment in helium of 0.04dex relative to solar is much larger than expected from first dredge-up at the base of the giant branch (e.g. Boothroyd & Sackmann 1999), considering that the initial abundance could be $\sim$ 0.085 to correspond to the low-Z environment. There is no clear explanation for this large helium abundance. If this were a consequence of third dredge-up, a correlation with carbon abundance would be expected, but this is not observed.

The mass of carbon brought to the surface of the star by third dredge-up and eventually expelled is four times the oxygen mass present. This is qualitatively in accordance with stellar evolution models which predict a more effective third dredge-up in low-Z stars (e.g., Marigo et al. 1999), as observationally confirmed in the Magellanic Clouds (e.g., Leisy & Dennefeld 1996). Adding up C+N+O (sum left unchanged by CNO bi-cycle) for Wray 16-423 and He 2-436 shows that the latter had 40% more dredge-up per hydrogen atom. The amount of

third dredge-up material may depend on the timing of the last thermal pulse(s). For low-mass stars, a few dredge-up episodes are responsible for most of the enrichment (*e.g.*, Wood 1997).

The nearly solar value of N/O in He 2-436 is in rough agreement with expectation as the initial N/O might have been of order one third the solar value in this moderate-*Z* galaxy and the predicted first-dredge-up enrichment of nitrogen is then by a factor 2-3 after "Cool Bottom Processing" (CBP, Boothroyd et al. 1999). The nitrogen 'enrichment' of Wray 16-423 (compared to He 2-436) points to a difference between the two PNe. Note that, with He/H = 0.108 and N/O = 0.22, Wray 16-428 is close to the edge of the PN Type I class, defined in the LMC as He/H > 0.105 and N/O > 0.3 (Torres-Peimbert & Peimbert 1997).

This nitrogen enrichment is on the order of the possible oxygen depletion (0.03dex) if both PNe originally had the same abundances. At temperatures above $2.5{\times}10^7$K, while the ON cycle reaches equilibrium, O is transformed into N. However, since the CN cycle first reaches equilibrium, nitrogen should already be much enriched before this can hold (*e.g.*, Smith et al. 1997). Alternatively, similar, relatively large nitrogen enrichment may have occured in both stars, nitrogen being then selectively converted into heavier elements, following high-temperature processing in the He 2-436 precursor under He-burning conditions (carbon is more abundant in He 2-436). However this interpretation is hampered by the fact the neon abundance appears to be almost the same in both PNe.

Finally, although nitrogen enrichment due to CNO burning of freshly synthesized carbon at the base of the convective envelope is normally restricted to massive AGB stars ("Hot Bottom Burning", *e.g.*, Blöcker & Schönberner 1991), the excess nitrogen in Wray 16-423 is a minute fraction of the carbon enrichment so that it possibly results from a transformation of carbon before third dredge-up.

In Table 7, average logarithmic abundance depletions <O, Ne>, <O, Ne, S>, <O, Ne, S, Ar> and <S, Ar> with respect to solar are given for the Sagittarius PNe. In Wray 16-423, all of these averages are obviously consistent with each other. The "best" averages, -0.575 ± 0.03 and -0.515 ± 0.04 for the old and new solar abundance sets respectively, are also consistent with the averages for all 7 elements (-0.54 ± 0.08 and -0.50 ± 0.07 respectively).

On the other hand, there seems to be a trend for increasing depletion with atomic number in He 2-436. The difference $\delta = $ <O, Ne> $-$ <S, Ar> is marginally significant for both solar sets ($\delta = 0.16 \pm 0.11$ and $\delta = 0.13 \pm 0.07$ resp.), although the interpretation may depend on the set used. Adopting the 1989 set, the depletion of sulfur is more pronounced but still compatible with those of oxygen and neon, with the stronger depletion of argon left as The argon abundance adopted in the He 2-436 models (Tables 3 and 5) is "conservatively large" since [Ar III] is correctly fitted and [Ar IV] overestimated (Table 4), then suggesting a genuine underabundance of argon, at least compared to

Table 7. Average depletions with respect to solar abundances

Elements	Wray 16-423 $-$ ⊙		He 2-436 $-$ ⊙	
	⊙ 89	⊙ 98	⊙ 89	⊙ 98
O, Ne	$-.57\pm.04$	$-.52\pm.02$	$-.56\pm.02$	$-.51\pm.05$
O, Ne, S	$-.57\pm.03$	$-.53\pm.04$	$-.59\pm.05$	$-.55\pm.09$
O, Ne, S, Ar	$-.58\pm.03$	$-.51\pm.05$	$-.64\pm.10$	$-.57\pm.08$
S, Ar	$-.59\pm.03$	$-.51\pm.09$	$-.72\pm.09$	$-.64\pm.02$

O and Ne. By contrast, adopting the 1998 set, an enrichment of O and Ne with respect to both S and Ar would be suggested.

Other combinations of depletions are possible however since there is no relationship between the decrease of, *e.g.*, the solar O and Ar abundance determinations from 1989 to 1998. Within quoted uncertainties of the 1998 solar abundances (± 0.06), the value of δ for He 2-436 can be reduced to less than 0.10 and yet our previous conclusion that depletions in Wray 16-423 are identical for all elements beyond nitrogen still apply. Since a $\delta < 0.10$ is manageable within the combined uncertainties arising from models (Table 6), it would be premature to conclude that S and/or Ar are "depleted" with respect to O and Ne in He 2-436. The suggestion concerning *solar* abundances is that the most consistent set of depletions is obtained in the Sagittarius PNe if O and Ar are intermediate between the 1989 and 1998 values and S close to the lower end of the range quoted in Table 6. Then all of the abundances available for oxygen and heavier elements in both PNe are consistent with a depletion of -0.55 ± 0.07. More specific conclusions require more definite reference abundances.

This re-analysis emphasizes the striking similarity of most abundances (excepting C and N) in both PNe. This "chemical homogeneity" is to be contrasted with the large abundance spread (0.7dex) implied by stellar studies (Mateo 1998). Also striking is the contrast with the wide range of abundances among Galactic Halo PNe (*e.g.*, Howard et al. 1997). Compared to Galactic PNe (Kingsburgh & Barlow 1994), a depletion ~ 0.4dex is obtained, but with large scatter (0.28 and 0.53dex for S and Ne respectively). However, considering the large discrepancy between the empirical and model S abundances in the case of the Sagittarius PNe (Table 6), doubts may be expressed about the reality of the low sulfur abundance of Galactic PNe, also based on empirical methods. The scatter would be reduced if this abundance was underestimated in the Galactic sample.

Despite the similarities shown by the two Sagittarius PNe, some differences are apparent. There is a *tendency* for oxygen to be more abundant in He 2-436 than in Wray 16-423, even though the error bars overlap (Péquignot et al. 2000). Also, the argon abundance looks unexpectedly smaller in He 2-436 than in Wray 16-423 (factor

Table 8. Central star properties

| | Wray 16-423 | | He 2-436 | |
	W97[a]	Models	W97[a]	Models
$T_{\rm eff}/10^3$K	$85-96$	107 ± 10	61	70 ± 10
$L_*/10^3 L_\odot$	2.3	$4.35\pm0.30^{[b]}$	5.3	$5.40\pm0.75^{[b]}$

[a] Walsh et al. (1997), Paper I
[b] The ±2 kpc uncertainty on the distance is not included.

1.5) and it is not clear how the model imperfections may gravely invalidate the significance of a direct comparison.

4.5. The nature of the nucleus of Wray 16-423

In Paper I, Wray 16-423 was classified as type [WC8] on the basis of the similar strengths of the broad [WR] features C III 465.0nm and C IV 580.6nm. This classification was puzzling, considering the high Zanstra temperature of the star, more than confirmed by the present models.

According to Paper I (Table 9, fluxes not de-reddened), the total flux of the $\lambda464.5$ blend in Wray 16-423 is 1.78 (H$\beta = 100$). Assuming a C IV intensity ratio $\lambda465.8/\lambda580.6$ as in He 2-436, the contribution of the [WR] feature C IV 465.8nm to the blend should be 0.21. Nebular line contributions are as follows. The Bowen fluorescence multiplet N III 463.4-4.2nm is ~ 0.91 (8% of He II 468.6nm, comparing to typical high-excitation PNe). The recombination multiplet C III 464.7-5.2nm is about twice as strong as C III 418.7nm (Table 2), or 0.27. The recombination multiplet O II 464.0-466.0nm is 0.24 (Table 2). The grand total is 1.63, which compares quite well with the observed flux.

Thus, within uncertainties, there is no need for a [WR] C III contribution to the $\lambda464.5$nm feature and Wray 16-423 can now be an early-type [WC], as expected. Higher resolution observations may re-inforce this contention.

4.6. Stars in the HR diagram

The central star properties turned out to be very similar in the HC and NEBU models (Sects. 3.3.3 ans 4.3.3) for both PNe. Effective temperatures $T_{\rm eff}$ and luminosities L_* are listed in Table 8 and compared to the empirical results of Paper I. The error bars are the sums of the uncertainties on modeling and absolute flux measurement, excluding (systematic) errors on the distance to the galaxy. L_*(Wray 16-423) is probably very accurate, owing to the perfect agreement of either the different absolute fluxes or the different model results. The new determination is significantly larger than the previous one, which had to rely on difficult continuum measurements and did not take into account the leakage of ionizing radiation. The uncertainty is larger for L_*(He 2-436), considering that (1) the radio flux predictions are sensitive to details of geometry (self-absorption), (2) helium is a problem in the HC model and

(3) the conversion of L_B (NEBU model) into L_* is not straightforward. The agreement with Paper I, based on the uncertain Hβ flux, is partly fortuitous.

The determination of L_* and $T_{\rm eff}$ allows the central stars to be placed on an HR diagram (Fig. 1). The theoretical evolutionary tracks plotted in Fig. 1 are taken from Vassiliadis and Wood (1994) using $Z = 0.004$, in accordance with the elemental abundances of the PNe. It was suggested in Paper I that the central stars were on He-burning tracks, as they showed [WC] spectral signatures and differed by a factor 2 in luminosity. The radio continuum data and the photoionization models showed that both luminosities L_* were in fact rather large and differed by a factor of only 1.24 ± 0.24, the smaller L_* of Wray 16-423 being explainable by its proximity to the turn-over. The positions of the stars on the HR diagram are now compatible with them being on H-burning tracks of initial masses $M = 1.19\pm0.08$ and 1.22 ± 0.14 $M_\odot$ for Wray 16-423 and He 2-436 respectively. Both stars may belong to the same evolutionary track. Then the weighted stellar-remnant mass is 0.61 $M_\odot$ and the initial mass:

$$M = (1.19\pm0.10)\ M_\odot.$$
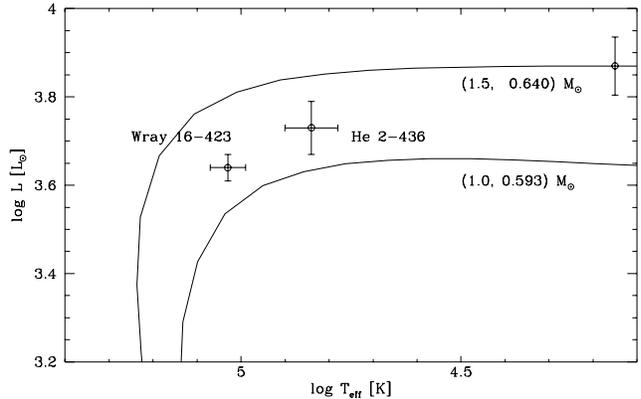
Fig. 1. HR diagram for Wray 16-423 and He 2-436 and evolutionary tracks for H-burning stars with $Z = 0.004$ according to Vassiliadis and Wood (1994). The error bar attached to the 1.5 $M_\odot$ track corresponds to the ±2 kpc uncertainty on the distance to Sagittarius.

For stars belonging to "standard" He-burning tracks of Vassiliadis and Wood (1994), the initial masses would be about 1.7 $M_\odot$, too large to be reconciled with AGB star properties in Sagittarius (Sect. 4.8). Evolutionary time scales are such however that definite tracks specific to helium burning may not be relevant (Boothroyd & Sackmann 1988; Blöcker 1995), whereas statistical analyses support the notion that H-burning-track luminosities may be more appropriate even for [WR] stars, at least in the Galaxy (e.g., Gorny 2000). Since the Sagittarius PN nuclei are probably He-burners, the genuine initial mass of both stars may be somewhat larger than in the above estimate.

4.7. Evolutionary status

The kinematic time scale of a PN may not faithfully reflect its "age", due to uncertainties on the pre-PN wind velocity and the different acceleration processes. Comparing directly the two PNe may provide a more reliable kinematic time. The average hydrogen density of Wray 16-423 is $<N_H> = 0.44 \times 10^4 cm^{-3}$. In He 2-436, assuming spherical symmetry for the outer shell (of which only 1/3 is currently illuminated due to shielding) and adding the mass of the inner shell, then $<N_H> = 2.7 \times 10^4 cm^{-3}$. The weighted average expansion velocities of He 2-436 and Wray 16-423 are $14.1 \, km \, s^{-1}$ and $25.5 \, km \, s^{-1}$ respectively (Gesicki & Zijlstra 2000). Assuming volume expansion with mean velocity $(14.1+25.5)/2 \, km \, s^{-1}$ from the present outer radius $\sim 1.1 \times 10^{17} cm$ of He 2-436, the density ratio of the PNe translates into a time scale $\Delta t_{kin} = 1430$ yr, with "final" radius $\sim 2.0 \times 10^{17} cm$. The actual average radius of Wray 16-423 is larger ($\sim 2.4 \times 10^{17} cm$) as more mass can be ionized owing to expansion. Meanwhile the dense inner shell of He 2-436, whose current kinematic time scale is probably less than 1000 yr, will fade considerably, as its density will decrease by a factor ~ 20, making He 2-436 look like Wray 16-423 at present.

The dynamic time scales of the stars are uncertain too. Given the core mass, the early post-AGB evolution is primarily sensitive to the poorly known mass loss rate. Although the evolutionary tracks of Vassiliadis & Wood (1994) are relevant to determine core and main-sequence masses (Fig. 1), their post-AGB wind strength may be underestimated (Wood 1997; Schönberner 1997). On the other hand, Blöcker (1995) probably overestimated mass loss rates during the early AGB evolution but tried to describe more realistically the decrease of mass loss as $T_{\rm eff}$ increases during post-AGB and his results are preferred for time scales. For core mass 0.61 $M_{\odot}$ and the large $T_{\rm eff}$'s relevant to the present PN nuclei, standard parametric mass losses apply, leading to $dT_{\rm eff}/dt \sim 25$K/yr for H-burning and a time scale $\Delta t_{dyn} = (1500 \pm 800)$ yr (the uncertainty arising mainly from the $T_{\rm eff}$ determinations), in accord with Δt_{kin}. Although the evolution of helium burners is sensitive to the epoch at which the fatal thermal pulse ignites, and there are no model tracks for such an evolution, the regime of $T_{\rm eff}$'s of interest here (in between the post-AGB and cooling phases) may be propitious to time scales relatively insensitive to details of the past history of the stars. Despite very large uncertainties, this coincidence of time scales re-inforces the analogy of these PNe.

The nucleus of He 2-436 is a [WC4] star (Paper I). This early type suggests an advanced stage of evolution, at variance with the *apparent* youth of the PN: the [O III]-weighted mean electron density N_e is over 10^5 cm^{-3}, met among Galactic PNe with [WR] central stars only for the latest possible type [WC11] (*e.g.*, Gorny 2000). Photoionization models show that the average N_e of He 2-436 is in fact a few 10^4 cm^{-3} (Sect. 4.7), alleviating the difficulty

(Galactic [WC4] stars have N_e up to 10^4 cm^{-3}). Wray 16-423, also excited by an early-type [WC] star, corresponds to the high-N_e end of Galactic counterparts.

4.8. Stellar population

The youngest stars in Sagittarius have ages around 5 Gyrs (Mateo 1998) which would give a mass of around 1.3 $M_{\odot}$, in fair agreement with the values above (Sect. 4.6). This coincidence of initial masses applies insofar as both PN nuclei have luminosities typical of H-burning or slightly lower. Star formation in dwarf galaxies is thought to occur in bursts (*e.g.*, Smecker-Hane et al. 1994), but the level of star formation in between is not well known. In view of the strong similarities of the abundances, little evolution of the ISM can have taken place between the formation of the two stars, which favours an origin within the same star formation burst in a well-mixed ISM.

The carbon stars in Sagittarius have well-determined magnitudes peaking at $M_{bol} = -4.5$ (Whitelock et al. 1996), corresponding to $L = 5 \times 10^3 \, L_{\odot}$, in extremely good agreement with the two PNe. Together with the high C/O of the PNe, this is strong evidence that the carbon stars form the source population of the PNe.

The abundances of the two PNe are independent of the age-metallicity degeneracy which affects photometric abundance determinations of the stellar population. They are therefore an excellent way of calibrating the photometric results. ¿From the AGB, Whitelock et al. (1996) estimated [Fe/H]=−0.8. Ibata et al. (1994) found a mean [Fe/H] of −1.1. Marconi et al. (1998) derived a metallicity range between −0.71 and −1.58. Sarajedini & Layden (1995) found several populations, the most metal-rich of which having [Fe/H] = −0.52. Only this last value corresponds to the PNe (−0.55 ± 0.07).

It should be noted that, from the slope of the giant branch, Whitelock et al. (1996) derived a larger abundance (−0.58) than the one they finally adopted. The difference was related to an assumption of a population age around 10^{10} yr. If a younger age is adopted, the AGB and PN abundances agree extremely well. It is therefore suggested that [Fe/H] of the AGB stars is in fact −0.58 rather than −0.8. The differences with other studies may be due to the age–metallicity degeneracy, the most metal-rich population of Sagittarius being somewhat younger than assumed in these studies. The presence of metal-poor populations is not in doubt, but the result of Sarajedini & Layden (1995) is confirmed regarding the most metal-rich population.

5. Conclusions

Abundances for the two PNe in the Sagittarius dwarf galaxy have been improved. The abundances of both PNe now appear remarkably similar for elements heavier than nitrogen. Abundances of nitrogen and carbon demonstrate the operation of the first and third dredge-ups. The larger

overabundance of carbon in He 2-436 is not unexpected as the total amount of third-dredge-up material may depend on the timing of the last thermal pulse(s). The excess nitrogen in Wray 16-423 is more intriguing, considering that second dredge-up does not occur in low-mass stars and helium is equally abundant in both objects. The large helium overabundance may be another problem.

The photoionization codes provide well-defined results for Wray 16-423 and a larger range of acceptable solutions for He 2-436. In the latter case, the unicity of solution breaks down, as a consequence of the high density in the inner shell. Line fluxes are matched within the 1-σ statistical errors, that is only a few percent for most basic lines, whilst the degrees of freedom are outnumbered by the independent observables.

Despite their [WC] spectra, both central stars delineate the 1.2 $M_\odot$ H-burning track, in fair agreement with the mass of the carbon stars of Sagittarius. The abundances of the PNe may help to calibrate the stellar photometry of the more metal-rich population in this galaxy.

Improving the absolute Hβ and radio fluxes for He 2-436 and, particularly, observing at radio frequencies above 9 GHz would more tightly constrain the geometry of the nebula and the luminosity of the nucleus, then leading to a more accurate mass of the star. Concerning Wray 16-423, the critical parameter to improve the positioning on the HR diagram is the effective temperature of the nucleus. Model atmospheres describing the ionizing FUV radiation from hot [WC] stars are needed.

The small angular size of the Sagittarius PNe allowed to secure global, reproducible spectra. The spectra obtained by Walsh et al. (1997) proved to be reliable in most of the optical range, as demonstrated by the overall excellent agreement between theory and observation for the H I and He I spectra (Table 6). They can however be usefully improved in the blue and near-UV and completed in the far-red and the UV. UV spectra are critical to check the energy balance and the carbon abundance of both PNe. New deeper optical observations are possible and highly desirable, considering that these objects represent a moderate-Z stellar population and appear as excellent test beds of models. Predictions for recombination line fluxes must be checked to ensure that these PNe are not subject to the same kind of discrepancy noted in some Galactic PNe between abundances obtained from collisional and recombination lines (*e.g.*, Liu et al. 1995).

References

Acker, A., Ochsenbein, F., Stenholm, B., et al., 1992, *Strasbourg-ESO Catalogue of Galactic Planetary Nebulae*

Anders, E., Grevesse, N., 1989, Geochim. Cosmochim. Acta 53, 197

Bedding, T.R., Zijlstra, A.A., 1994, A&A 283, 955

Blöcker, T., Schönberner, D., 1991, A&A 240, L11

Blöcker, T., 1995, A&A 299, 755

Boothroyd, A.I., Sackmann, I.-J., 1988, ApJ 328, 641

Boothroyd, A.I., Sackmann, I.-J., 1999, ApJ 510, 232

Brockelhurst, M., 1972, MNRAS 157, 211

Clegg, R.E.S., Harrington, J.P., 1989, MNRAS 239, 869

Clegg, R.E.S., Harrington, J.P., Barlow, M.J., Walsh, J.R., 1987, ApJ 314, 551

Clegg, R.E.S., Middlemass, D., 1987, MNRAS 228, 759

Crowther, P.A., Pasquali, A., De Marco, O., et al., 1999, A&A 350, 1007

Davey, A.R., Storey, P.J., Kisielius, R., 2000, A&AS, 142, 85

Feldmeier, A., Kudritzki, R.-P., Palsa, R., Pauldrach, A.W.A., Puls, J., 1997, A&A 322, 878

Ferland, G., Binette, L., Contini, M., et al., 1995, in *The Analysis of Emission Lines: A Meeting in Honor of the 70th Birthdays of D.E. Osterbrock & M.J. Seaton* Eds. R. Williams & M. Livio, Cambridge University Press, p. 83.

Gesicki, K., Zijlstra, A.A., 2000, A&A, 385, 1058

Gorny, S.K., 2000, in *Evolution and origin of [WC] stars*, in press

Grevesse, N., Lambert, D.L., Sauval, A.J., et al., 1991, A&A 242, 488

Grevesse, N., Sauval, A.J., 1998, Space Sci. Rev. 85, 161

Harrington, J.P., 1989, in *Planetary Nebulae*, IAU Symp. 131, ed. S. Torres-Peimbert, p. 157 (Kluwer)

Harrington, J.P., Seaton, M.J., Adams, S., Lutz, J.H., 1982, MNRAS 199, 517

Howard, J.W., Henry, R.B.C., McCartney, S., 1997, MNRAS 284, 465

Ibata, R.A., Gilmore, G., Irwin, M.J., 1994, Nature 370, 194

Ibata, R.A., Gilmore, G., Irwin, M.J., 1995, MNRAS 277, 781

Kingsburgh, R.L., Barlow, M.J., 1994, MNRAS 271, 257

Kono, A., Hattori, S., 1984, Phys. Rev. A 29, 2981

Kudritzki, R.P., Méndez, R.H., 1993, in *Planetary Nebulae*, IAU Symp. 155, eds. R. Weinberger & A. Acker, p. 47 (Kluwer)

Leisy, P., Dennefeld, M., 1996, A&AS 116, 95

Liu, X.W., Storey, P.J., Barlow, M.J., Clegg, R.E.S., 1995, MNRAS 272, 369

Marconi, G., Buonanno, R., Castellani, M., et al., 1998, A&A 330, 453

Marigo, P., Girardi, L., Bressan, A., 1999, A&A 344, 123

Mateo, L.M., 1998, ARA&A 36, 435

Mendoza, C., 1983, in *Planetary Nebulae*, IAU Symp. 131, ed. S. Torres-Peimbert, p. 143 (Kluwer)

Mendoza, C., Zeippen, C.J., 1982, MNRAS 198, 127

Morisset, C., Péquignot, D., 1996, A&A 312, 135

Nahar, S., 1995, ApJS 101, 423 (Erratum: ApJS 106, 213)

Nahar, S., 1999, ApJS 120, 131

Nahar, S., Pradhan, A.K., 1997, ApJS 111, 339

Péquignot, D., Petitjean, P., Boisson, C., 1991, A&A 251, 680

Péquignot, D., Zijlstra, A.A., Walsh, J.R., Dudziak, G., 2000, A&A Lett., in press

Petitjean, P., Boisson, C., Péquignot, D., 1990, A&A 240, 433

Ramsbottom, C.A., Bell, K.L., Keenan, F.P., 1997, MNRAS 284, 754

Ramsbottom, C.A., Bell, K.L., Keenan, F.P., 1999, MNRAS 307, 669

Robberto, M., Clampin, M., Ligori, S., Paresce, F., Staude, H.J., 1993, A&A 280, 241

Sarajedini, A., Layden, A., 1995, AJ 109, 1086

Sawey, J.M.K., Berrington, K.A., 1993, Atomic Data and Nuclear Tables 55, 81

Schönberner, D., 1997, in *Planetary Nebulae*, IAU Symp. 180, eds. H.J. Habing & H.J.G.L.M. Lamers, p. 379 (Kluwer)

Shaw, R.A., Dufour, R.J., 1995, PASP 107, 896

Smecker-Hane, T.A., Stetson, P.B., Hesser, J.E., Lehnert, M.D., 1994, AJ 108, 507

Smith, G.H., Shetrone, M.D., Briley, M.M., Churchill, C.W., Bell, R.A., 1997, PASP 109, 236

Smits, D.P., 1996, MNRAS 278, 683

Stasinska, G., Gorny, S.K., Tylenda, R., 1997, A&A 327, 736

Storey, P.J., 1994, A&A 282, 999

Storey, P.J., 1997, in *Planetary Nebulae*, IAU Symp. 180, eds. H.J. Habing & H.J.G.L.M. Lamers, p. 161 (Kluwer)

Storey, P.J., Hummer, D.G., 1995, MNRAS 272, 41

Torres-Peimbert, S., Peimbert, M., 1997, in *Planetary Nebulae*, IAU Symp. 180, eds. H.J. Habing & H.J.G.L.M. Lamers, p. 175 (Kluwer)

van Hoof, P., 2000, MNRAS 314, 99

Vassiliadis, E., Wood, P.R., 1994, ApJS 92, 125

Walsh, J.R., Dudziak, G., Minniti, D., Zijlstra, A.A., 1997, ApJ 487, 651 (Paper I)

Webster, B.L., 1983, PASP 95, 610

Whitelock, P.A., Irwin, M., Catchpole, R.M., 1996, New Astronomy 1, 57

Wood, P., 1997, in *Planetary Nebulae*, IAU Symp. 180, eds. H.J. Habing & H.J.G.L.M. Lamers, p. 297 (Kluwer)

Yamamoto, T.M., Sellmaier, F.H., Pauldrach, A.W.A., Hoffmann, T., 1997, in *Planetary Nebulae*, IAU Symp. 180, eds. H.J. Habing & H.J.G.L.M. Lamers, p. 135 (Kluwer)

Zijlstra, A.A., Walsh, J.R., 1996, A&A 312, L21

Zijlstra, A.A., Acker, A., Walsh, J.R., 1997, A&AS 125, 289

Table 2. Observations and model predictions for Wray 16-423

	HC			Observation		NEBU			
	Thin	Thick	Model	Flux	1σ Err	Thin	Thick	Model	Mod/Obs
Covering factors:	0.90	0.10	1.00			0.835	0.165	1.00	
Absolute fluxes									
log I_β (erg cm^{-2}s^{-1})	-11.89	-11.72	-11.87	-11.89	0.03	-11.93	-11.74	-11.89	1.00±.07
4.8 GHz (mJy)	4.5	6.7	4.8	4.72	0.10	4.35	6.37	4.69	0.99±.02
8.6 GHz (mJy)	4.3	6.4	4.5	4.31	0.10	4.12	6.12	4.45	1.03±.02
Relative line fluxes (wavelengths in nm)									
H I 486.1	100.00	100.00	100.00	100.00	-	100.00	100.00	100.00	-
Cont. 364.2 (/nm)	-	-	-	48.8	3.00	51.0	48.9	50.5	1.03±.06
Cont. 364.8 (/nm)	-	-	-	12.0	1.00	12.8	11.4	12.4	1.03±.08
H I 656.3	284.00	300.00	287.00	284.00	1.60	285.00	291.00	286.00	1.01±.01
He I 447.1	5.51	5.13	5.46	5.44	0.23	5.32	5.89	5.45	1.00±.04
He I 587.6	15.40	13.90	15.20	16.40	0.10	15.80	18.10	16.30	1.00±.01
He II 468.6	10.70	7.37	10.30	11.40	0.14	12.40	8.10	11.40	1.00±.01
C II 426.7	0.35	0.37	0.35	0.49	0.15	0.47	0.51	0.48	.98±.30
C III 418.7	-	-	-	<0.22	3σ	0.14	0.11	0.13	> 0.59
C III] 190.9+0.7	739.00	879.00	759.00	-	-	749.00	906.00	783.00	-
C IV 154.9	714.00	516.00	687.00	-	-	630.00	467.00	594.00	-
[N II] 658.4+4.8	11.40	103.00	24.30	22.70	0.16	8.31	70.80	22.90	1.01±.01
[N II] 575.5	0.25	2.12	0.51	0.53	0.05	0.16	1.51	0.48	.90±.10
[O I] 630.0+6.3	0.01	5.05	0.72	2.95	0.10	0.02	7.05	1.67	.56±.02
[O II] 372.6	11.20	77.50	20.40	20.30	0.40	12.50	47.70	20.70	1.02±.02
[O II] 372.9	4.57	32.60	8.57	8.84	0.27	5.85	17.80	8.65	.98±.03
[O II] 732.0+3.0	2.42	16.20	4.36	4.68	0.11	2.10	13.40	4.74	1.01±.02
O II 465.1+	-	-	-	<0.56	-	0.25	0.23	0.24	> 0.43
[O III] 500.7+495.9	1450.00	1340.00	1438.00	1460.00	6.00	1474.00	1415.00	1460.00	1.00±.00
[O III] 436.3	14.00	13.50	13.90	13.70	0.22	13.60	14.00	13.70	1.00±.02
[Ne III] 386.8+396.7	94.60	101.40	95.60	97.70	0.90	96.70	99.90	97.70	1.00±.01
Mg I] 457.1	-	-	-	0.31	0.10	0.25	0.50	0.31	1.00±.32
[S II] 671.6	0.33	6.86	1.25	1.53	0.09	0.84	3.80	1.53	1.00±.06
[S II] 673.1	0.58	11.20	2.08	2.86	0.07	1.41	7.36	2.80	.98±.02
[S II] 406.9	0.31	4.92	0.95	1.60	0.26	0.51	4.23	1.38	.86±.14
[S II] 407.6	0.10	1.60	0.31	0.54	0.18	0.16	1.37	0.45	.82±.27
[S III] 631.2	1.51	2.73	1.68	1.80	0.06	1.68	2.25	1.82	1.01±.03
[S III] 953.1+906.9	58.00	101.00	64.00	-	-	67.60	84.40	71.50	-
[Cl III] 551.7	-	-	-	0.25	0.04	0.24	0.26	0.25	.99±.15
[Cl III] 553.7	-	-	-	0.34	0.04	0.31	0.48	0.35	1.02±.12
[Ar III] 713.6+775.1	-	-	-	11.60	0.40	8.63	11.80	9.36	.80±.03
[Ar IV] 471.1	-	-	-	2.00	0.12	3.17	2.06	2.91	1.46±.09
[Ar IV] 474.0	-	-	-	2.90	0.08	3.44	3.22	3.39	1.17±.03
[Ar IV] 717.1+726.3+	-	-	-	0.33	0.10	0.26	0.25	0.26	.79±.24
[K IV] 610.2+679.5	-	-	-	0.17	0.05	0.17	0.15	0.17	1.00±.30
Line flux ratios									
[O II] 372.9/372.6	0.41	0.42	0.42	0.44	0.02	0.45	0.37	0.42	0.96±.04
[S II] 671.6/673.1	0.56	0.61	0.60	0.53	0.03	0.58	0.50	0.53	1.02±.06
[Cl III] 551.7/553.7	-	-	-	0.73	0.15	0.79	0.54	0.74	1.01±.20
[Ar IV] 471.1/474.0	-	-	-	0.69	0.05	0.92	0.64	0.86	1.24±.09
[N II] 658.4+/575.5	46.40	48.70	47.70	42.80	5.00	51.00	46.80	47.90	1.12±.13
[O II] 372.6+/732.0+	6.50	6.79	6.65	6.23	0.20	8.75	4.88	6.20	1.00±.03
[O III] 500.7+/436.3	104.00	99.50	103.00	107.00	1.70	108.00	101.00	107.00	1.00±.02
[S II] 671.6+/406.9+	2.24	2.78	2.63	2.05	0.42	3.35	1.99	2.37	1.16±.24
[Ar IV] 471.1+/717.1+	-	-	-	14.90	4.60	25.20	20.90	24.40	1.64±.50

Table 4. Observations and model predictions for He 2-436

	HC	Observation		NEBU			
	Model	Flux	1σ Err	High N_H	Low N_H	Model M2	M2/O
Covering factors:				0.624	0.376	1.000	-
Absolute fluxes							
$\log I_\beta (\mathrm{erg\ cm^{-2}s^{-1}})$	-11.57	-11.59	0.06	-11.65	-11.65	-11.65	0.88±.13
1.46 GHz (mJy)	0.5	0.62	0.25	0.32	3.10	1.36[a]	2.20±.90
4.89 GHz (mJy)	3.7	3.90	0.20	2.97	6.81	4.41[a]	1.13±.06
8.40 GHz (mJy)	6.1	4.90	0.20	4.95	6.89	5.68[a]	1.16±.05
Relative line fluxes (wavelengths in nm)							
H I 486.1	100.00	100.00	-	100.00	100.00	100.00	-
Cont. 364.2 (/nm)	-	43.6	3.50	44.7	48.5	46.1	1.06±.08
Cont. 364.8 (/nm)	-	6.80	0.70	6.00	8.90	7.10	1.05±.10
H I 656.3	288.00	288.00	1.6	289.00	289.00	289.00	1.00±.01
He I 447.1	5.85	6.07	0.21	6.07	5.93	6.02	.99±.03
He I 587.6	16.00	18.50	0.17	18.90	18.20	18.60	1.01±.01
He II 468.6	0.16	<0.7	-	0.47	0.48	0.48	> 0.64
C II 426.7	0.79	0.96	0.22	0.97	0.87	0.93	.97±.22
C III 418.7	-	<0.50	3σ	0.07	0.14	0.10	> 0.20
C III] 190.9+0.7	1210.00	-	-	1150.00	912.00	1060.00	-
C IV 154.9	715.00	-	-	166.00	233.00	191.00	-
[N II] 658.4+4.8	7.67	14.30	0.75	9.01	22.20	14.00	.98±.05
[N II] 575.5	0.54	1.11	0.09	1.49	0.57	1.15	1.03±.08
[O I] 630.0+6.3	0.88	6.83	0.09	4.08	3.73	3.95	.58±.01
[O II] 372.6	3.29	8.25	0.90	2.82	19.90	9.23	1.12±.12
[O II] 372.9	1.01	3.08	0.86	0.84	6.66	3.02	.98±.27
[O II] 732.0+3.0	5.93	13.60	0.12	15.90	9.61	13.50	.99±.01
O II 465.1+	-	<5.00	-	0.26	0.27	0.27	> 0.05
[O III] 500.7+495.9	1090.00	1065.00	6.00	959.00	1237.00	1063.00	1.00±.01
[O III] 436.3	14.00	14.20	0.30	16.80	9.76	14.20	1.00±.02
[Ne III] 386.8+396.7	77.00	75.30	1.70	77.90	71.00	75.30	1.00±.02
Mg I] 457.1	-	<0.39	3σ	0.35	0.23	0.30	> 0.79
[S II] 671.6	0.39	0.50	0.03	0.14	1.14	0.51	1.03±.06
[S II] 673.1	0.82	1.13	0.03	0.32	2.39	1.10	.97±.03
[S II] 406.9	2.24	2.36	0.55	3.28	2.33	2.93	1.24±.29
[S II] 407.6	0.69	0.82	0.43	0.99	0.76	0.90	1.10±.57
[S III] 631.2	1.10	2.52	0.04	3.16	1.57	2.57	1.02±.02
[S III] 953.1+906.9	68.00	-	-	62.50	66.20	63.90	-
[Cl III] 551.7	-	<0.24	3σ	0.03	0.13	0.07	> 0.27
[Cl III] 553.7	-	<0.24	3σ	0.12	0.34	0.20	> 0.84
[Ar III] 713.6+775.1	-	8.12	0.30	8.70	6.44	7.85	.97±.04
[Ar IV] 471.1	-	0.22	0.19	0.15	0.79	0.39	1.79±1.5
[Ar IV] 474.0	-	0.74	0.14	1.02	1.87	1.34	1.81±.35
[Ar IV] 717.1+726.3+	-	<0.35	3σ	0.20	0.13	0.17	> 0.48
[K IV] 610.2+679.5	-	<0.24	3σ	0.07	0.05	0.06	> 0.25
Line flux ratios							
[O II] 372.9/372.6	0.31	0.37	0.11	0.30	0.33	0.33	0.87±.27
[S II] 671.6/673.1	0.48	0.44	0.03	0.43	0.47	0.47	1.06±.07
[Ar IV] 471.1/474.0	-	0.29	0.24	0.14	0.42	0.29	1.00±.80
[N II] 658.4+/575.5	14.20	12.90	1.20	6.04	38.90	12.20	.94±.09
[O II] 372.6+/732.0+	0.73	0.83	0.13	0.23	2.77	0.91	1.09±.16
[O III] 500.7+/436.3	77.60	75.00	1.60	57.00	127.00	75.00	1.00±.02
[S II] 671.6+/406.9+	0.20	0.51	0.16	0.11	1.14	0.42	.82±.26

[a] No shielding between sectors included (see Sect. 3.4.2).

Table 5. Helium lines[a]

λ (nm)	Wray 16-423 He/H = 0.1074			He 2-436 He/H = 0.1041 (M) and 0.1072 (M')				Comments[b]
	O	M	M/O	O	M	M/O	M'/O	
He I triplet (with $2^3S - n^3P$ self-absorption)								
706.52	7.31	9.77	1.340±.015	13.18	12.81	.972±.016	.912±.015	
388.86	7.97	8.00	.996±.034	7.59	7.59	1.000±.070	1.016±.070	H I subtr.
587.57	16.37	16.33	.998±.006	18.48	18.63	1.009±.009	1.000±.009	
471.32	.55	1.05	(1.910±.160)	1.26	1.25	1.002±.130	1.052±.140	[Ar IV] subtr. using λ474.0nm
447.15	5.44	5.45	1.003±.043	6.07	6.02	.993±.034	1.001±.034	and predicted doublet ratio
412.08	< .65	.36	> .560	.29	.42	1.420±.300	1.370±.300	
402.62	2.72	2.46	.904±.084	3.41	2.68	.790±.135	.798±.135	He II and weak He I subtr.
381.96	1.27	1.34	1.055±.210	1.19	1.46	1.230±.400	1.240±.400	
370.50	0.61	0.82	1.340±.600	–	–	–	–	H I subtr.
He I singlet (Case B)								
728.13	.82	1.14	1.392±.073	1.10	1.34	1.216±.028	1.172±.028	Case A ∼ B/1.8
667.82	3.99	3.97	.995±.043	4.57	4.41	.964±.011	.977±.011	
504.77	.21	.23	1.093±.270	< .25	.26	> 1.040	> 1.020	Case A ∼ B/1.4
396.47	.54	1.32	2.440±2.00	.86	1.41	1.630±2.00	1.670±2.00	Case A ∼ B/30, [Ne III] subtr.
492.19	1.33	1.34	1.010±.052	1.64	1.47	.896±.070	.915±.071	
443.76	< .21	.08	> .360	< .23	.08	> .370	> .360	Case A ∼ B/1.3
361.36	< 1.37	.64	> .470	–	–	–	–	Case A ∼ B/25
438.79	.74	.62	.839±.113	.50	.67	1.340±.300	1.370±.300	

[a] Observed dereddened fluxes (O) and model fluxes (M) in units Hβ = 100.
[b] "Case A ∼ B/2" means that, under Case A conditions, the predicted line intensity would be half the Case B value.

Table 6. Comparison of abundances[*]

Elem.	Wray 16-423 W97[c]	Models	He 2-436 W97[c]	Models	Galactic PNe[a]	Solar[b]⊙ AG89/GS98	Wray − ⊙	He 2 − ⊙	GPNe − ⊙
H	12.00	12.00±.00	12.00	12.00±.00	12.00±.00	12.00	-	-	-
He	11.03	11.03±.01	11.02	11.03±.01	11.05±.03	10.99	0.04	0.04	0.06
C	8.83	8.86±.06	9.18	9.06±.09	8.81±.30	8.60/8.52	0.26/0.34	0.46/0.54	0.21/0.29
N	7.62	7.68±.05	6.97	7.42±.06	8.14±.20	8.05/7.92	−.37/−.24	−.63/−.50	0.09/0.22
O	8.31	8.33±.02	8.29	8.36±.06	8.69±.15	8.93/8.83	−.60/−.50	−.57/−.47	−.24/−.14
Ne	7.50	7.55±.03	7.57	7.54±.06	8.10±.15	8.09/8.08	−.54/−.53	−.55/−.54	0.01/0.02
Mg	-	6.98±.30	-	-		7.58	−.60:	-	-
S	6.48	6.67±.04	6.30	6.59±.05	6.91±.30	7.24±.06	−.57	−.65	−.33
Cl	-	4.89±.18	-	-		5.28	−.39:	-	-
Ar	5.88	5.95±.07	5.76	5.78±.08	6.38±.30	6.56/6.40	−.61/−.45	−.78/−.62	−.18/−.02
K	-	4.65±.22	-	-		5.13	−.48:	-	-

[*] Abundances are given on a logarithmic scale where H = 12
[a] Mean composition and scatter for non-Type I Galactic PNe (Kingsburgh & Barlow 1994)
[b] AG89 = Anders & Grevesse (1989), except for C (Grevesse et al. 1991); GS98 = Grevesse & Sauval (1998)
[c] Walsh et al. (1997), Paper I